# Dimension Engineering of High-Quality InAs Nanostructures on a Wafer Scale

Dong Pan,[†,#] Ji-Yin Wang,[‡] Wei Zhang,[§,¶] Lujun Zhu,[∥,▲] Xiaojun Su,[§] Furong Fan,[‡] Yuhao Fu,[⊥] Shaoyun Huang,[‡] Dahai Wei,[†] Lijun Zhang,[⊥] Manling Sui,[∥] Arkady Yartsev,[§] Hongqi Xu,[‡,▽,◇] and Jianhua Zhao[*,†,#,◆,◇]

[†]State Key Laboratory of Superlattices and Microstructures, Institute of Semiconductors, Chinese Academy of Sciences, P.O. Box 912, Beijing 100083, China

[‡]Beijing Key Laboratory of Quantum Devices, Key Laboratory for the Physics and Chemistry of Nanodevices and Department of Electronics, Peking University, Beijing 100871, China

[§]NanoLund and Division of Chemical Physics, Lund University, Box 124, 22100 Lund, Sweden

[∥]Institute of Microstructure and Properties of Advanced Materials, Beijing University of Technology, Beijing 100124, China

[⊥]Key Laboratory of Automobile Materials of MOE and School of Materials Science and Engineering, Jilin University, Changchun 130012, China

[#]Center of Materials Science and Optoelectronics Engineering, University of Chinese Academy of Sciences, Beijing 100190, China

[▽]NanoLund and Division of Solid-State Physics, Lund University, Box 118, S-22100 Lund, Sweden

[◇]Beijing Academy of Quantum Information Sciences, Beijing 100193, China

[◆]CAS Center for Excellence in Topological Quantum Computation, University of Chinese Academy of Sciences, Beijing 100190, China
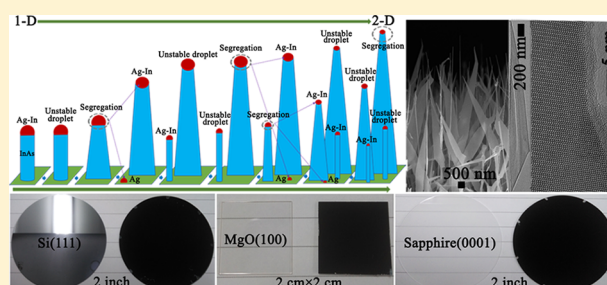
[¶]School of Physics and Electronic Engineering, Guangzhou University, Guangzhou 510006, China

[▲]College of Physics and Information Technology, Shaanxi Normal University, Xi'an 710062, China

**S** *Supporting Information*

**ABSTRACT:** Low-dimensional narrow-band-gap III−V semiconductors are key building blocks for the next generation of high-performance nanoelectronics, nanophotonics, and quantum devices. Realizing these various applications requires an efficient methodology that enables the material dimensional control during the synthesis process and the mass production of these materials with perfect crystallinity, reproducibility, low cost, and outstanding electronic and optoelectronic properties. Although advances in one- and two-dimensional narrow-band-gap III−V semiconductors synthesis, the progress toward reliable methods that can satisfy all of these requirements has been limited. Here,



we demonstrate an approach that provides a precise control of the dimension of InAs from one-dimensional nanowires to wafer-scale free-standing two-dimensional nanosheets, which have a high degree of crystallinity and outstanding electrical and optical properties, using molecular-beam epitaxy by controlling catalyst alloy segregation. In our approach, two-dimensional InAs nanosheets can be obtained directly from one-dimensional InAs nanowires by silver−indium alloy segregation, which is much easier than the previously reported methods, such as the traditional buffering technique and select-area epitaxial growth. Detailed transmission electron microscopy investigations provide solid evidence that the catalyst alloy segregation is the origination of the InAs dimensional transformation from one-dimensional nanowires to two-dimensional nanosheets and even to three-dimensional complex crosses. Using this method, we find that the wafer-scale free-standing InAs nanosheets can be grown on various substrates including Si, MgO, sapphire, GaAs, etc. The InAs nanosheets grown at high temperature are pure-phase single crystals and have a high electron mobility and a long time-resolved terahertz kinetics lifetime. Our work will open up a conceptually new and general technology route toward the effective controlling of the dimension of the low-dimensional III−V semiconductors. It may also enable the low-cost fabrication of free-standing nanosheet-based devices on an industrial

*continued...*

scale.

Low-dimensional narrow-band-gap III−V semiconductor InAs is an ideal material for applications in high-speed and low-power electronics, infrared optoelectronics, and quantum-transport studies because it exhibits high electron mobility, a narrow band gap, and strong spin−orbit coupling.[1−3] For example, the well-grown one-dimensional (1-D) InAs nanowires have been used to fabricate single-electron transistors, resonant tunneling diodes, and ballistic transistors.[4−6] Recently, it has
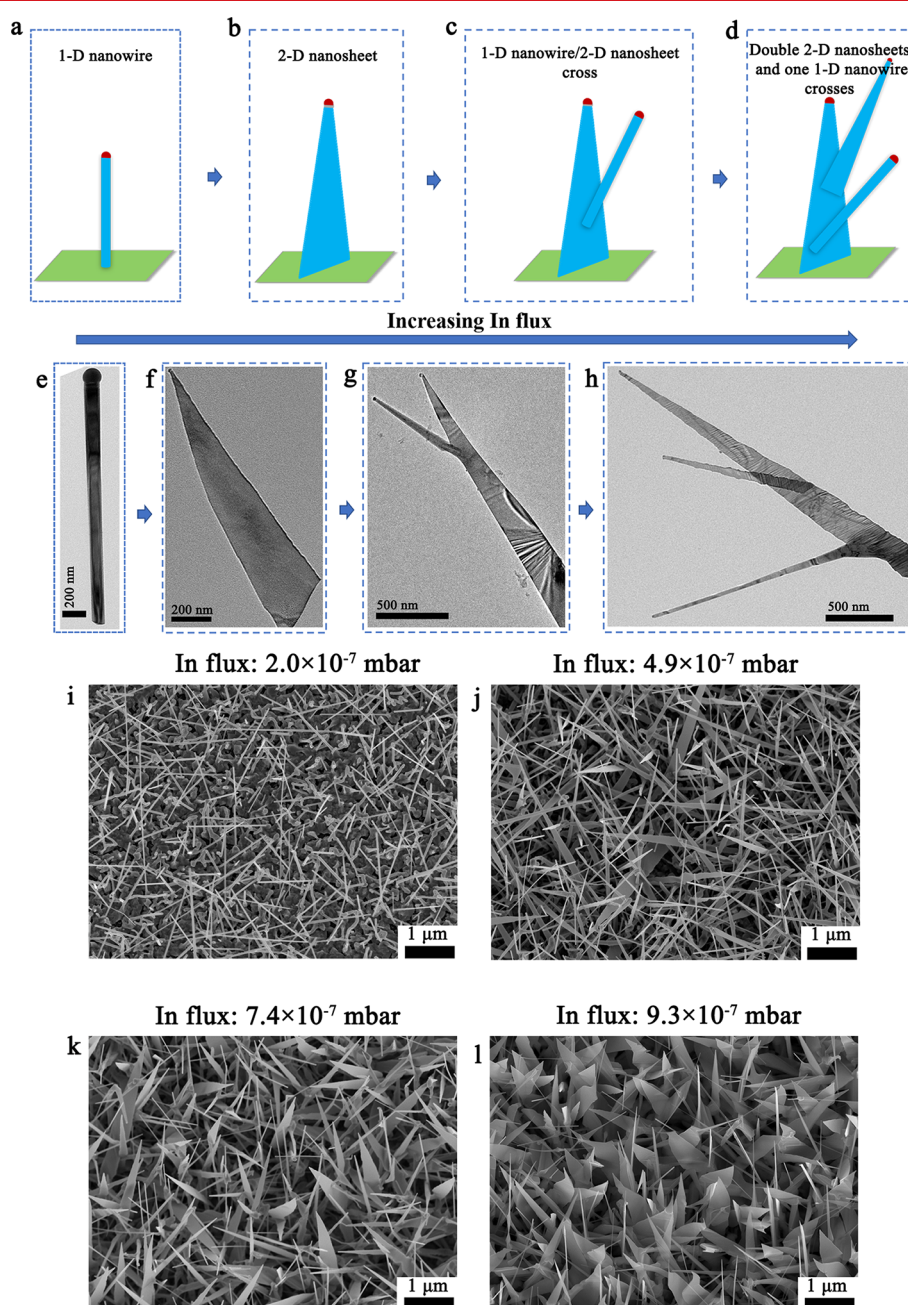


**Figure 1.** Dimensional tunability of InAs from 1-D nanowires to 2-D nanosheets and to 3-D complex crosses by increasing the indium flux. (a−d) Schematic illustration of InAs with the morphology tuned from (a) a 1-D nanowire to (b) a 2-D nanosheet, to (c) a 1-D nanowire/2-D nanosheet cross, and to (d) double 2-D nanosheets and one 1-D nanowire crosses by increasing the indium flux. (e−h) TEM images of a typical 1-D nanowire, 2-D nanosheet, 1-D nanowire/2-D nanosheet cross, and double 2-D nanosheets and one 1-D nanowire crosses, respectively. (i−l) The 25° tilted SEM images of InAs nanostructures grown at different indium fluxes (keeping the arsenic flux constant, $5.9 \times 10^{-6}$ mbar) on Si (111) substrates using silver as catalysts. By increasing the indium flux (indium fluxes in panels i−l are $2.0 \times 10^{-7}$, $4.9 \times 10^{-7}$, $7.4 \times 10^{-7}$, and $9.3 \times 10^{-7}$ mbar, respectively), the dimension of InAs can be tuned directly from 1-D to 2-D. For all of the samples, the growth time is 40 min, and the growth temperature is 505 °C.
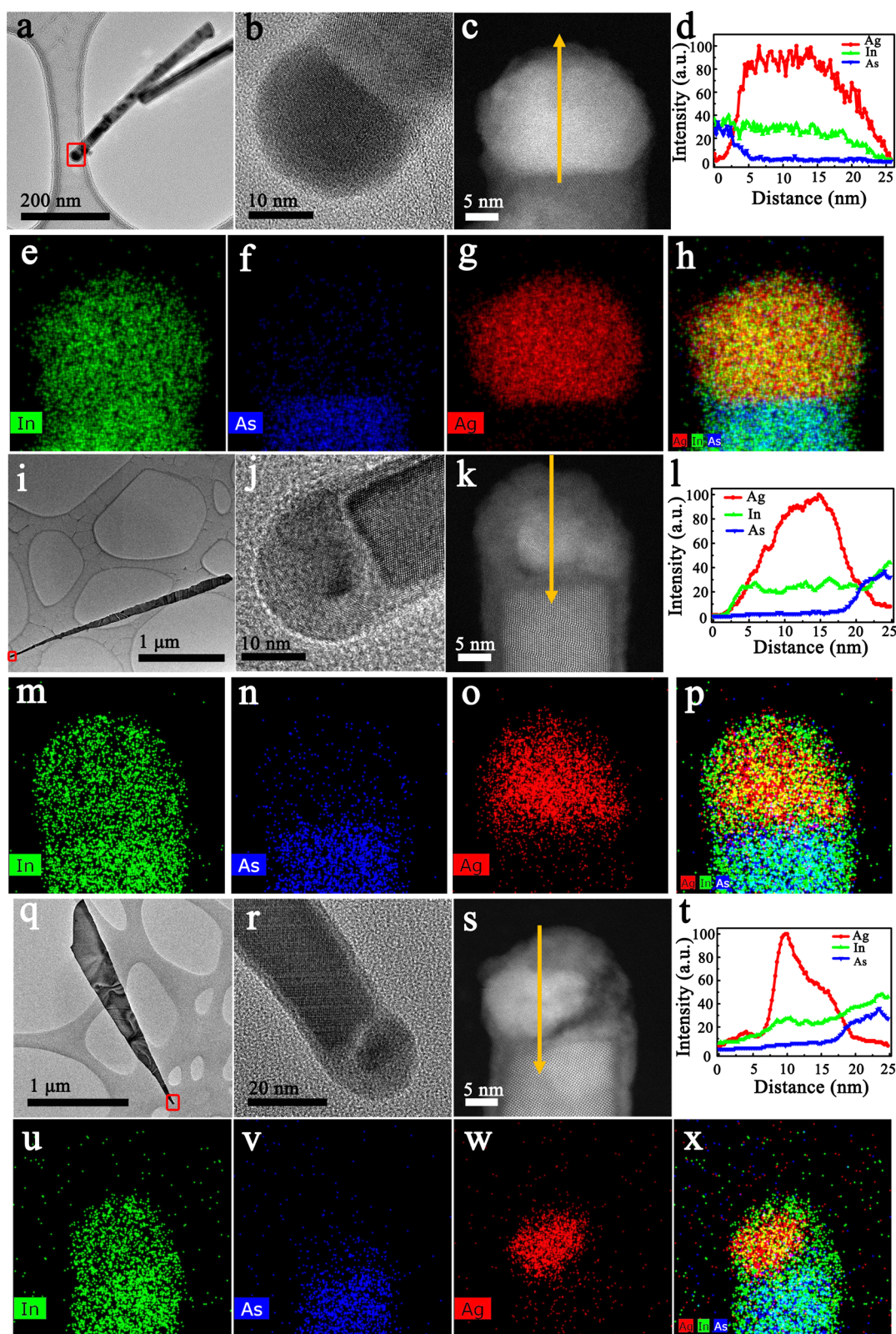
**Figure 2.** Crystal structure and elemental distribution of catalyst alloy particle of the InAs with the dimensional evolution from 1-D to 2-D. (a−c, i−k, q−s) TEM, high-resolution TEM and HAADF-STEM images taken from the InAs nanostructures grown with the indium flux of $2.0 \times 10^{-7}$, $4.9 \times 10^{-7}$, and $7.4 \times 10^{-7}$ mbar, respectively. The red rectangles in panels a, i, and q highlight the regions where the high-resolution TEM images were recorded. (e−h, m−p, u−x) False-color EDS elemental maps taken at the top region of the InAs nanostructures in panels c, k, and s, respectively. (d, l, t) EDS line scans taken along the axial direction (marked with yellow arrows) of the catalyst alloy particle in panels c, k, and s, respectively.

also been successfully used to detect the Majorana Fermions in tunable semiconductor and superconductor hybrid devices.[7−11]

In contrast to 1-D InAs nanowires, free-standing InAs nanosheets present another class of two-dimensional (2-D)

material, where the band structure can be precisely tuned from bulk to 2-D by changing the thickness.[12] Its structural configuration also enables the direct contact of the active semiconductor layer with the gate stack, which is essential for enabling high-performance devices.[13] Very recently, 2-D InAs also shows great prospect in braiding or interferometric measurement on topological quantum computing.[14] All of these applications require a high degree of InAs growth control on its morphology and especially dimension. Conventionally, a complex buffer layer engineering was used to grow 2-D InAs structures. Several reports have also been published on obtaining the 2-D GaAs nanosheets and InAs membranes and nanoleaves by a modified epitaxial transfer scheme,[12,15] select area epitaxial growth,[16−19] and the mirror-twin-induced method.[20] However, the ability of these techniques to realize wafer-scale growth and well-controlled dimension modulation remains limited.

Here, we report a general method for growth of wafer-scale free-standing 2-D InAs nanosheets with controllable nanoscale dimensions, a high degree of crystallinity and outstanding electrical and optical properties using molecular-beam epitaxy (MBE) by catalyst alloy segregation. Our 2-D InAs nanosheets can be obtained directly from 1-D InAs nanowires by silver−indium alloy segregation, which is independent of buffer-layer engineering. The wafer-scale free-standing InAs nanosheets can be grown on various substrates including Si, MgO, sapphire, GaAs, etc. The InAs nanosheets grown at high temperature are pure-phase single crystals and have a high electron mobility and a long time-resolved terahertz (THz) kinetics lifetime. The growth method presented here not only provides a general and conceptually new approach for controlling the dimension of the low-dimensional III−V semiconductors but also enables the low-cost fabrication of free-standing nanosheet-based devices on an industrial scale.

All InAs nanostructures were grown in a solid source MBE system (VG 80) using silver as seed particles. For catalyst deposition, we used a silver effusion cell attached to the III−V growth chamber. This configuration enabled us to deposit the catalyst on a chemically clean surface and at the same time to control the substrate temperature and monitor the deposition process with reflection high-energy electron diffraction. The conventional one step catalyst annealing process was used to generate silver nanoparticles as reported in our previous work.[21] Commercial p-type Si (111), MgO (100), polished and unpolished sapphire (0001), and GaAs (100) were used as the substrates. Before loading the substrates into the MBE chamber, they were cleaned and treated using different methods (see Supporting Information section S1) to remove the surface contamination or native oxide. Samples were grown with V/III beam equivalent pressure (BEP) ratios from 3.0 to 29.5 (by increasing the indium flux while keeping the arsenic (As$_4$) flux constant) for 40 min at 505 °C in the variant indium flux series (see Supporting Information sections S2 and S3). Samples were grown for time from 2.5 to 80 min with a V/III BEP ratio of 6.3 at 505 °C in the variant growth time series (see Supporting Information sction S5). The detailed growth conditions of the 2-D InAs nanosheets grown using "catalyst alloy segregation" with a two-step growth procedure and the 2-D InAs nanosheets grown on MgO (100), sapphire (0001), and GaAs (100) substrates were summarized in Supporting Information sections S9 and S10, respectively. Samples were grown at temperatures from 420 to 545 °C for 40 min and with a V/III BEP ratio of 6.3 in the variant growth temperature series (see Supporting Information section S11). All of the InAs nanostructure growth

was terminated by switching off the indium supply while maintaining the arsenic supply until the substrate was cooled down below 300 °C within a few minutes.

For electrical and optical measurements, the detailed device fabrications and device parameters of the 2-D InAs nanosheets were provided in Supporting Information section S14, and the time-resolved THz measurements were conducted by a setup described in Supporting Information section S1.

**Dimensional Tunability of InAs from 1-D to 2-D.** We find that the dimension of InAs can be tuned directly from 1-D nanowires to 2-D nanosheets and even to 3-D complex crosses, and the indium flux is the only determined parameter for the dimensional tunability. Figure 1a−d is the schematic illustration of InAs with the morphology tuned from a 1-D nanowire (Figure 1a) to a 2-D nanosheet (Figure 1b), to a 1-D nanowire/2-D nanosheet cross (Figure 1c) and to double 2-D nanosheets and one 1-D nanowire crosses (Figure 1d) by increasing the indium flux. Figure 1e−h shows corresponding typical transmission electron microscope (TEM) images for these different dimensional InAs nanostructures. Detailed morphology evolution process of InAs from 1-D to 2-D can be clearly observed from the samples grown at different indium fluxes (keeping the arsenic flux, growth temperature, and growth time constants) on Si (111) substrates by MBE using silver as catalysts. As shown in Figure 1i, for the sample grown with the indium flux of 2.0 × 10$^{-7}$ mbar, InAs nanowires are obtained on the substrate surface. Increasing the indium flux slightly up to 4.9 × 10$^{-7}$ mbar, sheet-like InAs nanostructures appear (Figure 1j). Further increasing the indium flux to 7.4 × 10$^{-7}$ mbar, the resulting InAs nanostructures have obvious sheet morphology (Figure 1k). By increasing the indium flux to 9.3 × 10$^{-7}$ mbar, high-density and large-size (length and width are both in the micrometer scale) free-standing 2-D InAs nanosheets are obtained (Figure 1l). At last, for the sample grown with a higher indium flux, 3-D complex InAs crosses appear. InAs planar epitaxial layers form on the substrates for the samples grown with a very low V/III BEP ratio (see Supporting Information section S2). It is worth noting that the density of the 2-D InAs nanosheets increases remarkably with increasing the indium flux. Because the indium flux is the only parameter for the dimensional tunability, the dimensional transformation of InAs from 1-D to 2-D and to 3-D should originate from the same crystal growth mechanism.

**Catalyst Alloy Segregation Growth Model.** As we observed in Figure 1, the dimension of InAs can be tuned directly from 1-D nanowires to 2-D nanosheets and to 3-D complex crosses just by tailoring the indium flux. To find the reason for the dimensional evolution of InAs, spherical aberration-corrected (Cs-corrected) high-angle annular dark-field scanning transmission electron microscopy (HAADF-STEM) and energy-dispersive X-ray spectroscopy (EDS) mapping were performed on the InAs samples grown with different indium fluxes using an FEI Titan G2 microscope equipped with a super-X detector. For the sample grown with the indium flux of 2.0 × 10$^{-7}$ mbar, TEM results further confirm that the sample is nanowires. As can be seen from Figure 2a, InAs nanowires have homogeneous diameter, and spherical catalyst alloy particles at the end of the InAs nanowires can be clearly observed. High-resolution TEM and HAADF-STEM images of the spherical catalyst alloy particle indicate that the alloy particle is fully single-crystalline (Figure 2b,c). EDS maps (Figure 2e−h) and line scan (Figure 2d) taken at the top region of the nanowire indicate that the remaining spherical catalyst particle is composed of silver and indium, and their elemental distributions
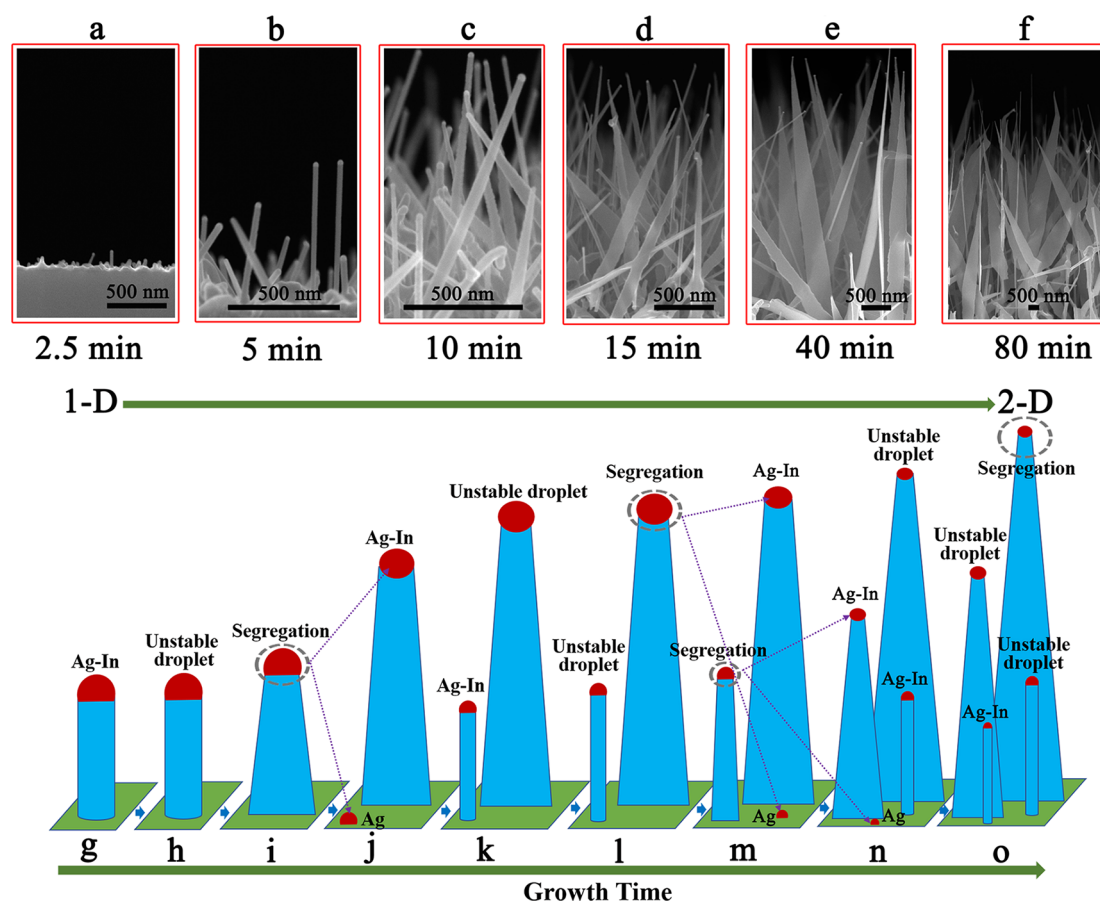
**Figure 3.** Experimental results of the InAs grown under the same indium-rich conditions with different growth times and a schematic demonstration of the catalyst alloy segregation process for the dimensional evolution of InAs from 1-D to 2-D. (a−f) Side-view SEM images of InAs grown on Si (111) substrates for 2.5, 5, 10, 15, 40, and 80 min, respectively. For all of the samples, the V/III BEP ratio is 6.3 (indium and arsenic fluxes are $9.3 \times 10^{-7}$ and $5.9 \times 10^{-6}$ mbar, respectively), and the growth temperature is 505 °C. (g−o) Schematic illustrating the catalyst alloy segregation process. (g) An InAs nanowire with a spherical silver−indium alloy droplet on its top. (h) The silver−indium alloy droplet becomes unstable under an indium-rich growth condition. (i) The silver−indium alloy droplet starts segregation, and the morphology of InAs evolves from 1-D nanowire to 2-D nanosheet gradually. (j) The silver−indium alloy droplet finishes segregation, and the segregated silver droplet in panel i migrates to the substrate surface. (k) The silver−indium alloy droplet on the 2-D nanosheet becomes unstable, and the segregated silver droplet seeds a new InAs nanowire growth. (l) The silver−indium alloy droplet on the 2-D nanosheet starts segregation again, and the silver−indium alloy droplet on the new 1-D InAs nanowire becomes unstable. (m) Silver−indium alloy droplet on the 2-D nanosheet finishes segregation and the segregated silver droplet in panel l migrates to the substrate surface. The silver−indium alloy droplet on the new 1-D InAs nanowire starts segregation, and the morphology of the new InAs evolves from 1-D nanowire to 2-D nanosheet gradually. (n, o) Silver−indium alloy droplets undergo the same segregation process in panels g−m, and high-density 2-D InAs nanosheets form on the substrate.

are already slightly inhomogeneous in comparison with the samples grown with lower indium fluxes (see Figure S2). As shown in Figure 2i, increasing the indium flux slightly up to $4.9 \times 10^{-7}$ mbar, InAs has a sheet-like morphology, which is consistent with the scanning electron microscope (SEM) image in Figure 1j. It is noteworthy that the spherical catalyst alloy particle is not single-crystal anymore according to the high-resolution TEM and HAADF-STEM results in Figure 2j,k. EDS maps (Figure 2m−p) and line scan (Figure 2l) taken at the top region of the InAs further indicate that the distribution of the silver atoms becomes inhomogeneous. Figure 2q is a typical TEM image of an InAs nanosheet grown with the indium flux of $7.4 \times 10^{-7}$ mbar. From the high-resolution TEM and HAADF-STEM results in Figure 2r,s, we can see that the catalyst alloy particle is polycrystalline, and the inhomogeneous distribution of the silver atoms in the catalyst alloy is more obvious. This phenomenon can be further confirmed by EDS maps (Figure 2u−x) and the line scan (Figure 2t). For the sample grown with the indium flux of $7.4 \times 10^{-7}$ mbar or higher, pure silver nanoparticles segregate

from the catalyst alloy of InAs, and they can be clearly observed and detected from the STEM images and EDS point analysis (see Supporting Information section S3). For the samples grown with a lager indium flux, thin indium shells form on the surface of catalyst alloy particles and InAs nanosheets (Figure 2h,p,x). A similar phenomenon was also observed in the InAs nanostructures catalyzed by other metal nanoparticles.[22] Our results confirm that the indium-rich condition plays an important role in the dimensional transformation of InAs.

Because the indium-rich condition is the only requirement for the catalyst alloy segregation as well as the dimensional evolution of InAs from 1-D to 2-D, the catalyst alloy segregation process appeared in the samples grown with different indium fluxes (Figures 2a−x, S2, and S3) should be observed for a sample grown under the indium-rich condition at different growth stages. To further figure out the catalyst alloy segregation process for the dimensional evolution of the InAs from 1-D to 2-D, a set of InAs samples have been grown under the same indium-rich growth condition with different growth time. Figure
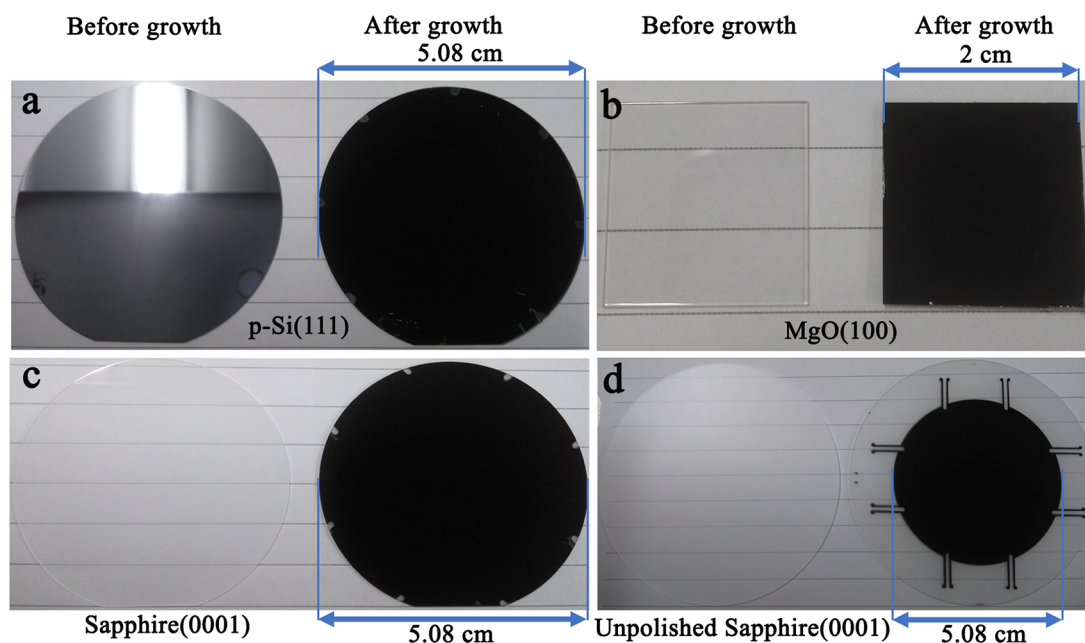
**Figure 4.** Wafer-scale 2-D InAs nanosheets grown on various substrates. (a−d) The 2-D InAs nanosheets grown on 2 in. p-Si (111), 2 cm × 2 cm MgO (100), 2 in. sapphire (0001), and 3 in. (the substrate window is 2 in.) unpolished sapphire (0001) substrates, respectively. Left and right images for each panel are the substrates images taken before and after sample growth with the camera of the Redmi 5 Plus, respectively.

3a−f is side-view SEM images of InAs grown on Si (111) substrates for 2.5, 5, 10, 15, 40, and 80 min, respectively. As shown in Figure 3a, the sample grown for 2.5 min, the InAs is the 1-D nanowires and their lengths are from several tens of nanometers to 100 nm. Extending the growth time to 5 min, the length of InAs increases to about 500 nm, and the morphology of InAs is still the 1-D nanowire with a homogeneous diameter (Figure 3b), but the droplets on the top of nanowires are very unstable (see Supporting Information section S4). When the growth time is increased to 10 min, it can be found that the length of InAs nanowires further increases. However, the nanowires have an obviously lateral growth trend (Figure 3c). Further increasing the growth time to 15 min, sheet-like InAs can be observed (Figure 3d). For even longer growth time (40 min), larger-scale high-density free-standing 2-D nanosheets are grown on the substrate (Figure 3e and Supporting Information section S5). When the growth time is extending to 80 min, 2-D nanosheets with a larger scale, super-high density, free-standing characteristics, and lager size (length and width can be up to 10 and 2 $\mu$m, respectively) are obtained, as observed in Figure 3f. The density of the 2-D nanosheets on the substrate surface increases with increasing sample growth time, which indicates that the indium-rich growth condition is very suitable for the 2-D nanosheet growth, as we observed in Figure 1i−l. For this series of InAs samples, detailed TEM, HAADF-STEM, and EDS results confirm that the catalyst alloy on top of InAs has undergone the same segregation process (see Supporting Information section S6) as that in the InAs samples grown with the different indium fluxes in Figure 1.

According to above results, we believe that the dimensional evolution of InAs from 1-D to 2-D is oriented from the catalyst alloy segregation under indium-rich growth conditions. The schematic demonstration of the catalyst alloy segregation process under indium-rich conditions is given in Figure 3g−o. First, if InAs is grown under indium-poor growth conditions or located at the initial stage of the growth as shown in Figure 3a (the value of indium flux is smaller than the value that can

produce an unstable droplet), the morphology is 1-D nanowire with a single crystal spherical silver−indium alloy droplet on its top (Figure 3g). At these growth conditions, the interface between nanowire and catalyst alloy nanoparticle is sharp as that in the III−V semiconductor nanowires seeded by other metals[23,24] due to the isotropical growth of the nanowires. Then, when the growth atmosphere of InAs is gradually becoming indium-rich by increasing the indium flux (or increasing the growth time in a large indium flux), the silver−indium alloy droplet will become unstable, and the distribution of the silver atoms becomes inhomogeneous (Figure 3h). As soon as the indium-rich growth condition is reached, the silver−indium alloy droplet starts segregation, and the morphology of InAs evolves from 1-D nanowire to 2-D nanosheet gradually due to the anisotropical growth caused by catalyst alloy segregation (Figure 3i). As the growth and segregation proceeds, the silver−indium alloy droplet finishes segregation and the segregated silver droplet can migrate to the substrate surface as shown in Figure 3j (if the silver droplet migrates onto the surface of nanosheet, the sample will transform from 1-D nanowires to 3-D complex crosses; see Supporting Information section S7). The interface between 2-D nanosheet and the catalyst alloy nanoparticle is not sharp anymore owing to the above anisotropical growth. After that, the silver−indium alloy droplet on the 2-D nanosheet becomes unstable, and the segregated silver droplet seeds a new InAs nanowire growth (Figures 3k and S10). As the growth continues, the silver−indium alloy droplet on the 2-D nanosheet starts segregation again, and the silver−indium alloy droplet on the new 1-D InAs nanowire also becomes unstable (Figure 3l). Next, as can be seen from Figure 3m, the silver−indium alloy droplet on the 2-D nanosheet finishes segregation and the segregated silver droplet can also migrate to the substrate surface. The silver−indium alloy droplet on the new 1-D InAs nanowire also starts segregation, and the morphology of the new InAs evolves from 1-D nanowire to 2-D nanosheet gradually. After that, silver−indium alloy droplets continuously undergo the same segregation process shown in
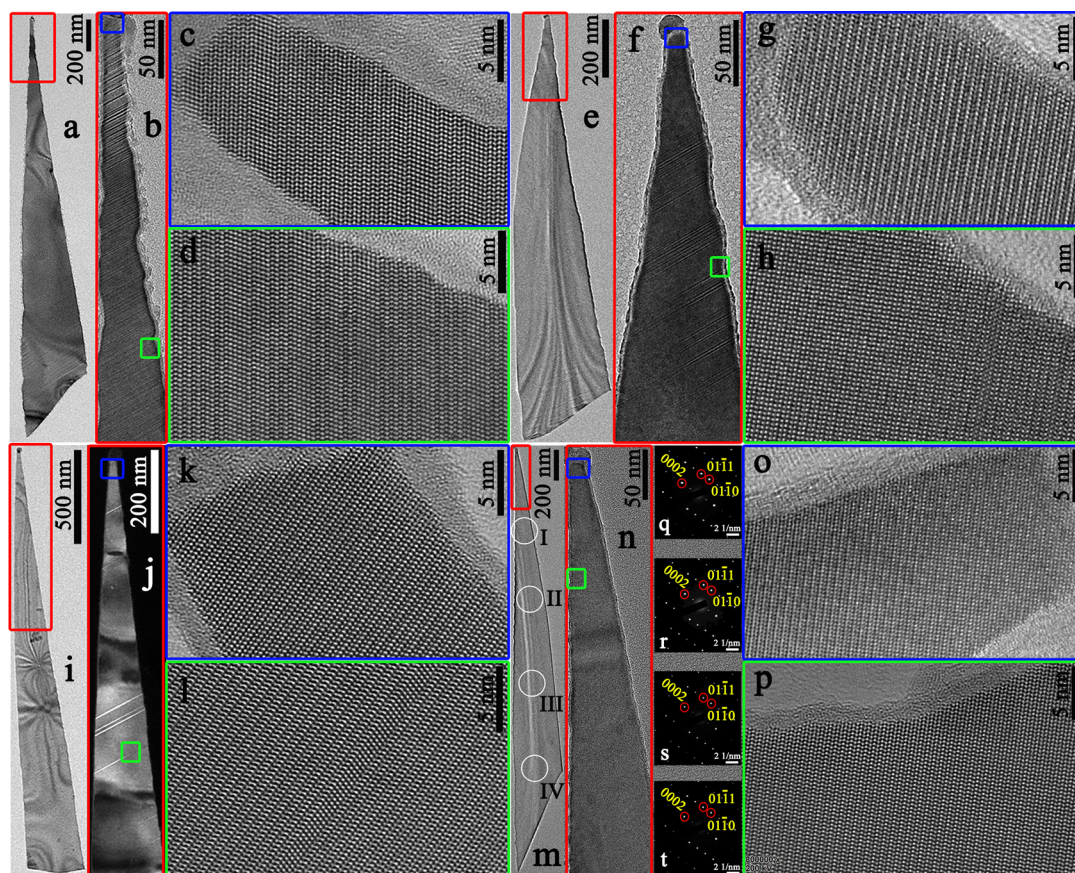
**Figure 5.** Influence of temperature on 2-D InAs nanosheet crystal-phase purity. (a−d) TEM results of a typical InAs nanosheet grown at 475 °C. (a) The overview TEM image of the nanosheet. (b−d) High-resolution TEM images taken from different regions of the InAs nanosheet. (e−h) TEM images of a typical InAs nanosheet grown at 505 °C. (e) Overview TEM image of the nanosheet. (f−h) High-resolution TEM images taken from different regions of the InAs nanosheet. (i−l) TEM images of a typical InAs nanosheet grown at 525 °C. (i) The overview TEM image of the nanosheet. (j) A dark-field TEM image taken in the top section in the nanosheet. (k, l) High-resolution TEM images taken from different regions of the InAs nanosheet. (m−t) TEM and SAED results of a typical InAs nanosheet grown at 545 °C. (m) The overview TEM image of the nanosheet. (n−p) High-resolution TEM images taken from different regions of the InAs nanosheet. (q−t) SAED patterns taken along the $[2-1-10]$ axis from regions I, II, III, and IV, respectively. The white circles highlight the regions where SAED patterns were recorded. All of the rectangles in panels a−n highlight the regions where the high-resolution TEM images were recorded.

Figure 3g−m, and high-density 2-D InAs nanosheets (Figure 3n,o) form on the substrate. The catalyst alloy segregation takes place in all the samples grown with different V/III BEP ratios as long as the growth conditions are indium-rich. For samples grown under the same large indium flux for different growth time, the growth condition will also become indium-rich more and more with increasing the growth time. The more the indium-rich condition, the faster the segregation process. That is why we have observed the dimension of InAs can be tuned directly from 1-D to 2-D, and the density of the 2-D InAs nanosheets increase remarkably with increasing indium flux (Figure 1) or growth time (Figure 3). With continuation of the segregation process, the volume of the droplets deduces gradually. Thus, very thin 2-D InAs nanosheets can be obtained in our samples. In the Supporting Information section S8, we have provided a more-detailed discussion on the possible growth mechanism of the InAs nanostructures in our study.

**Generality and Scope of Catalyst Alloy Segregation Crystal Growth.** We find that the tuning the dimension of the low-dimensional III−V semiconductors by the catalyst alloy segregation is a general method. For example, we can realize the dimensional tunability of InAs from 1-D to 2-D using "catalyst alloy segregation" with a two-step growth procedure. In the so-

called two-step growth process, InAs nanowires are first grown on the substrate with silver as catalysts and then tuning the growth conditions to "indium-rich" (after InAs nanowire growth, increasing the indium flux to a large value and keeping other parameters constant) to ensure that the catalyst alloy segregation can happen. It is found that the high-density and large-size 2-D InAs nanosheets can still be obtained (see Supporting Information section S9).

Another very important characteristic for the "catalyst segregation crystal growth" is that wafer-scale free-standing 2-D InAs nanosheets can be realized by this method on various substrates with different size including Si, MgO, sapphire and GaAs, etc. Figure 4a−d shows the typical top view substrate images taken before and after sample grown on the 2 in. p-type Si (111), 2 cm × 2 cm MgO (100) and 2 in. polished and 3 in. unpolished sapphire (0001) substrates, respectively. As shown in Figure 4a, Si (111) substrate has a clean surface (like a mirror) before the 2-D InAs nanosheet growth. In contrast, the substrate has a very homogeneous black surface after sample growth. MgO (Figure 4b) and sapphire (Figure 4c,d) substrates are transparent before the sample growth, while they are all homogeneous black in color after sample growth. Interestingly, 2-D InAs nanosheets are not sensitive to the substrates surface,
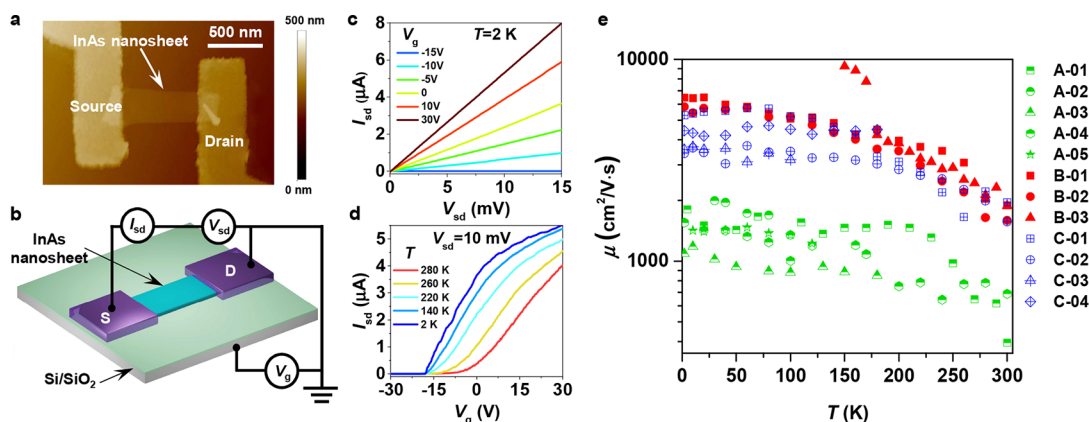
**Figure 6.** Transport characteristics of the InAs nanosheet devices. (a) AFM image of device B-01. (b) Schematic diagram of an InAs nanosheet device. A bias voltage $V_{sd}$ is applied on the source with the drain grounded. A back-gate voltage $V_g$ is applied to tune the electron density in InAs nanosheet. (c) Output characteristic curves of device B-01 at different back-gate voltages at $T = 2$ K. (d) Transfer characteristic curves of device B-01 as a function of back-gate voltage $V_g$ at different temperatures with $V_{sd} = 10$ mV. (e) Extracted mobility of InAs nanosheet devices at different temperatures by fitting transfer characteristic curves. Labels A−C correspond to devices made from InAs nanosheet grown in different conditions. For A devices, InAs nanosheets are grown at 455 °C with a V/III BEP ratio of 6.3. For B devices, the growth temperature is increased to 545 °C, and the V/III BEP ratio is fixed at 6.3. For C devices, InAs nanosheets are grown at 505 °C with a V/III BEP ratio of 5.4.

as can be seen from Figure 4c,d, samples grown on the polished and unpolished sapphire (0001) substrates both have homogeneous color. Detailed highly amplified SEM images indicate that 2-D InAs nanosheets have very homogeneous density and distribution in the different area of all these substrates (see Supporting Information section S10). Here, the dimensional tunability of wafer-scale InAs from 1-D to 2-D at various substrates with different size can be expected substantially to reduce the cost of producing high-quality low-dimensional InAs and may enable the low-cost fabrication of InAs-based devices on an industrial scale.

**Phase Purity of 2-D InAs Nanosheets.** As to the crystal structure of the 2-D InAs nanosheets, the nanosheets are composed of a mixture of wurtzite (WZ) and zinc-blende (ZB) segments (Figure 2j,k,r,s), as reported in most III−V 1-D nanowires and 2-D nanomembranes grown with a bottom-up manner.[25,16] These effects might have an impact on the nanosheets' optical and electrical properties and may pose problems in future nanoelectronic devices due to electron scattering at stacking faults or twin planes.[26,27] Careful control of the structure of III−V nanomaterials will improve the success of future devices, including heterostructure devices. In our work, 2-D InAs nanosheets can be grown well with a large substrate temperature range (see Supporting Information section S11). Luckily, we find that phase-pure 2-D InAs nanosheets can be achieved by only varying the growth temperature. Figure 5 are the typical TEM images of InAs nanosheets grown at different temperatures. For nanosheets grown at 475 °C (Figure 5a), the structure is a mixture of WZ and ZB phases. As shown in Figure 5b−d, stacking faults and twin defects can be clearly observed from the HRTEM images taken from top and side regions in the nanosheet. In Figure 5e−h, it is observed that the density of single stacking faults is obviously reduced for the nanosheet grown at 505 °C. Further increasing the growth temperature to 525 °C (Figure 5i), we can see that the density of stacking faults is strongly reduced. The number of the stacking faults is countable using the dark-field TEM (Figure 5j) and HRTEM images (Figure 5k,l). At high growth temperatures (e.g., 545 °C), selected-area electron diffraction (SAED, Figure 5q−t) patterns and HRTEM images (Figure 5o,p) confirm that nanosheets have high crystal quality with only one or nearly no

stacking faults and other defects along their entire length (see Supporting Information section S12). As shown in Figure 6 below, the electrical transport measurements confirm the result that raising growth temperature could improve the quality of InAs nanosheets. Our results are in accordance with the previous report that a high growth temperature coupled with a low V/III BEP ratio (indium-rich conditions) produced pure WZ nanowires free of stacking faults.[28,29] We find that the V/III BEP ratio (indium flux in this work) is not very sensitive to the crystal quality of the 2-D InAs nanosheets. As shown in Figure 2, the structures are all composed with WZ and ZB mixture phases with the indium fluxes increasing from $4.9 \times 10^{-7}$ to $9.3 \times 10^{-7}$ mbar. To our surprise, if we further increasing the indium flux to $1.1 \times 10^{-6}$ mbar (V/III = 5.4), the crystal-quality can be much improved even for the sample grown at a low temperature (505 °C; see Supporting Information dection 13). Electrical measurements shown in Figure 6 are also consistent with our HRTEM results and confirm that further increasing indium flux can help improve crystalline quality of InAs nanosheets. Phase purity achieved without sacrificing important specifications of size and dopant level opens new possibilities for engineering nanosheet devices without restrictions on nanosheet size or doping.

**Electrical and Optical Properties of 2-D InAs Nanosheets.** To access the electronic properties of the grown InAs nanosheets, we have performed transport measurements on nanosheet devices. It is noted that in this paper, we have measured three kinds of devices labeled A−C, in which the used InAs nanosheets are grown in three different conditions. For A devices, InAs nanosheets are grown at 455 °C with a V/III BEP ratio of 6.3. For B devices, the growth temperature is increased to 545 °C, and the V/III BEP ratio is fixed at 6.3. For C devices, InAs nanosheets are grown at 505 °C with a V/III BEP ratio of 5.4. Figure 6a shows the atomic force microscopy (AFM) image of device B-01. In the device, the source and drain electrodes are fabricated by depositing 5 nm titanium and 90 nm gold. Details about the fabrication processes and device geometries are shown in Supporting Information section 14. As shown in Figure 6b, a bias voltage $V_{sd}$ is applied on the source with drain grounded and the carrier density in InAs nanosheet is tuned by back-gate voltage $V_g$. Figure 6c shows the output characteristic curves of
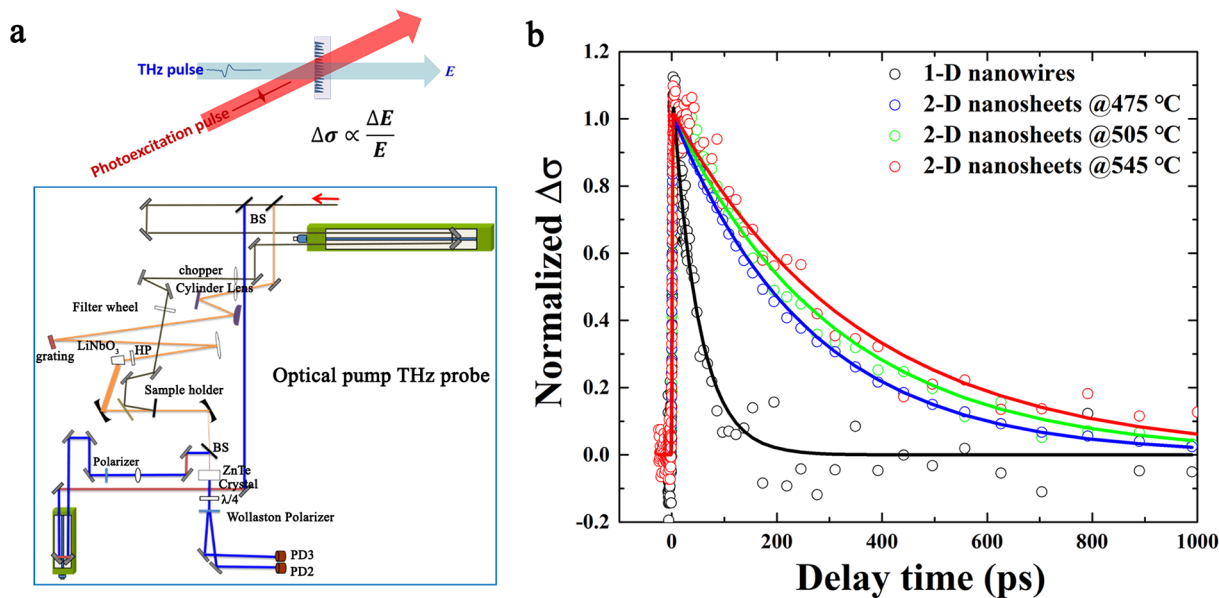
**Figure 7.** Optical properties of 1-D InAs nanowires and 2-D InAs nanosheets. (a) The setup for the time-resolved THz measurements. (b) TRTS kinetics of 1-D InAs nanowires (black circle) and 2-D InAs nanosheets grown at 475 °C (blue circle), 505 °C (green circle), and 545 °C (red circle) after photoexcitation at 1.55 eV. The excitation photon flux is ~$2 \times 10^{12}$ cm$^{-2}$. The solid lines are the fitting curves by using single exponential decay functions.

device B-01 at different back-gate voltages at $T = 2$ K. The linear output curves indicate that the device possesses ohmic contact between electrodes and nanosheet even at a low temperature. Figure 6d depicts transfer characteristic curves of device B-01 with $V_{sd} = 10$ mV at different temperatures. The device behaves as a typical n-type field-effect transistor. We find that with decreasing temperature the transconductance becomes steeper implying that electron mobility is improved. By fitting the transfer characteristic curves (see the details in Supporting Information section S15), we can extract field-effect mobility of the InAs nanosheet devices as shown in Figure 6e. By comparing A devices with B devices, we find that B devices possess much higher electron mobility globally at all accessible temperatures, indicating that the InAs nanosheets of B devices possess much higher crystalline quality than that of A devices. The results are consistent with the TEM and SAED results shown in Figure 5 and section 12 of Supporting Information that increasing growth temperature can improve the crystalline quality of InAs nanosheets. In Figure 6e, we observe that at room temperature the electron mobility of B devices is about ~2000 cm$^2$/V·s, much larger than other uncapsuled two-dimensional material such as layered MoS$_2$[30] and black phosphorus.[31] At $T = 10$ K, the electron mobility of the group B devices can reach to ~7000 cm$^2$/(V s), almost as high as that found in free-standing 2-D InSb nanostructures.[32,33] Besides, in Figure 6e we find that the mobility of C devices is nearly close even if not as high as that of B devices, implying that the crystalline quality of InAs nanosheets grown at low temperatures can be improved by further reducing the V/III BEP ratio, which is consistent with the TEM results in Supporting Information section 13. Such high-quality 2-D nanosheets can work as a building block for constructing scalable high-performance nanoelectronic and quantum devices in the future.

Time-resolved THz spectroscopy (TRTS) is selectively sensitive to photoconductivity of the samples, which is proportional to the product of mobility and concentration of photogenerated charges. Consequently, TRTS kinetics can be used to analyze carrier recombination processes as well as mobility dynamics. In planar InAs, electron mobility is significantly higher than that of holes;[34,35] thus, we presume that photoconductivity is mainly arising from photogenerated electrons. In InAs nanosheets, the photoconductivity ($\Delta\sigma$) dynamics can be described by the following rate equation:[36]

$$\frac{d(\Delta\sigma)}{dt} = e\mu_e(t) \times \left( -AN(t)^3 - \gamma N(t)^2 - \frac{N(t)}{\tau_{\text{e-trap}}} \right)$$

where $\mu_e(t)$ is the electron mobility; $N$ is the concentration of electrons; $A$ and $\gamma$ are the rates of the Auger and bimolecular recombination, respectively; and $1/\tau_{\text{e-trap}}$ is the electron trapping rate. TRTS kinetics of InAs nanosheets with varied growth temperatures were measured by the setup described in Figure 7a. As shown in the Figure 7b, the $\Delta\sigma$ decays of 1-D nanowires and 2-D nanosheets can be fitted by single exponential decay functions, suggesting that TRTS kinetics are dominated by monomolecular recombination processes such as electron trapping.[36] The fitted lifetimes for 1-D nanowires is $49.7 \pm 4.8$ ps, while those for 2-D nanosheets are $258.9 \pm 7.8$, $310.2 \pm 13.6$, and $354.4 \pm 23.8$ ps for samples grown at 475 °C (blue circle), 505 °C (green circle), and 545 °C (red circle), respectively. Apparently, the $\Delta\sigma$ lifetime of 2-D nanosheets is much longer than that of 1-D nanowires and gradually increases with the growth temperature. In high-crystallinity semiconductors, electron mobility does not change with time; thus, the variation of the lifetime is caused by different charge trapping. Therefore, slower decay of photoconductivity can be attributed to the reduced trap density in the nanosheets with increasing growth temperature. In 2-D InAs nanosheets, both the surface and bulk traps can contribute to the electron trapping processes. To understand the nature of traps, we examined SEM and TEM of the samples. From SEM and TEM images, we find that the overall geometric structure and indium-rich shell of nanosheets grown at 475, 505, and 545 °C are similar. Accordingly, we would expect that the impacts of surface status on carrier lifetime

of nanosheets are similar for the samples grown at varies temperatures, and TRTS decays are most likely dominated by electron bulk traps, which decrease with increasing sample growth temperature. These results agree with TEM measurements and electrical characterizations above.

In summary, we demonstrate a new and general strategy for realizing the wafer-scale dimensional tunability of low-dimensional III−V semiconductors. Wafer-scale free-standing 2-D InAs nanosheets with controlled dimensions, a high degree of crystallinity, and outstanding electrical and optical properties have been obtained using MBE by the catalyst alloy segregation. The catalyst alloy segregation can be used to tune the InAs from 1-D nanowires to 2-D nanosheets and even to 3-D complex crosses. The wafer-scale free-standing 2-D InAs nanosheets can be grown on various substrates including Si, MgO, sapphire, GaAs, etc. The phase purity of 2-D InAs nanosheets can be achieved for the sample grown at high temperatures. These pure-phase single-crystal InAs nanosheets have a high electron mobility and a long time-resolved THz kinetics lifetime. Although in this work, we have, respectively, focused on InAs and silver as the semiconductor and catalyst, other compound semiconductors and metal catalysts could be explored in the future. The proposed nanosheet growth mechanism could be general to many materials. The reported wafer-scale and potentially high-throughput method can be expected substantially to reduce the cost of producing high-quality nanosheets and may enable the low-cost fabrication of nanosheet-based devices on an industrial scale. At the moment, our results cannot be fully explained by the existing literature, and we expect these results to inspire the development of new theoretical models.

## ASSOCIATED CONTENT

### Ⓢ Supporting Information

The Supporting Information is available free of charge on the ACS Publications website at DOI: 10.1021/acs.nanolett.8b04561.

Details on substrate treating procedures and equipment for sample characterization, dimensional tunability, structural characteristics chemical compositions, unstable silver−indium alloy droplets, InAs samples grown under the same indium-rich growth condition for different growth times, the transformation process of InAs from a 1-D nanowire to 3-D complex nanocrosses, a possible growth mechanism of the 2-D InAs nanosheets, dimensional tunability, wafer-scale free-standing 2-D InAs nanosheets , the temperature growth window for 2-D InAs nanosheets, crystal quality, device fabrications and device parameters, and extraction of field-effect mobility of InAs nanosheet devices (PDF)

## AUTHOR INFORMATION

### Corresponding Author
*E-mail: jhzhao@red.semi.ac.cn.

### ORCID Ⓞ
Lijun Zhang: 0000-0002-6438-5486
Arkady Yartsev: 0000-0003-4941-4848
Hongqi Xu: 0000-0001-6434-2569
Jianhua Zhao: 0000-0003-2269-3963

### Author Contributions
D.P. and J.H.Z. designed the experiments. D.P. grew all of the samples and did all of the SEM measurements. D.P., L.J.Z., and M.L.S. analyzed the structures and compositions using TEM and EDS. J.Y.W., F.R.F., S.Y.H., and H.Q.X. fabricated the devices, performed the electrical measurements, and analyzed the electrical data. W.Z., X.J.S., and A.Y. performed the optical measurements and analyzed the optical data. Y.H.F., D.H.W., and L.J.Z. carried out theoretical calculations. D.P. and J.H.Z. wrote the manuscript. All authors discussed the results and commented on the manuscript.

### Notes
The authors declare no competing financial interest.

## REFERENCES

(1) del Alamo, J. A. Nanometre-scale electronics with III-V compound semiconductors. *Nature* **2011**, *479*, 317.

(2) Tomioka, K.; Yoshimura, M.; Fukui, T. A III-V nanowire channel on silicon for high-performance vertical transistors. *Nature* **2012**, *488*, 189.

(3) Pettersson, H.; Trägårdh, J.; Persson, A. I.; Landin, L.; Hessman, D.; Samuelson, L. Infrared photodetectors in heterostructure nanowires. *Nano Lett.* **2006**, *6*, 229.

(4) Thelander, C.; Mårtensson, T.; Björk, M. T.; Ohlsson, B. J.; Larsson, M. W.; Wallenberg, L. R.; Samuelson, L. Single-electron transistors in heterostructure nanowires. *Appl. Phys. Lett.* **2003**, *83*, 2052.

(5) Björk, M. T.; Ohlsson, B. J.; Thelander, C.; Persson, A. I.; Deppert, K.; Wallenberg, L. R.; Samuelson, L. Nanowire resonant tunneling diodes. *Appl. Phys. Lett.* **2002**, *81*, 4458.

(6) Chuang, S.; Gao, Q.; Kapadia, R.; Ford, A. C.; Guo, J.; Javey, A. Ballistic InAs nanowire transistors. *Nano Lett.* **2013**, *13*, 555.

(7) Das, A.; Ronen, Y.; Most, Y.; Oreg, Y.; Heiblum, M.; Shtrikman, H. Zero-bias peaks and splitting in an Al-InAs nanowire topological superconductor as a signature of Majorana fermions. *Nat. Phys.* **2012**, *8*, 887.

(8) Krogstrup, P.; Ziino, N. L. B.; Chang, W.; Albrecht, S. M.; Madsen, M. H.; Johnson, E.; Nygård, J.; Marcus, C. M.; Jespersen, T. S. Epitaxy of semiconductor-superconductor nanowires. *Nat. Mater.* **2015**, *14*, 400.

(9) Albrecht, S. M.; Higginbotham, A. P.; Madsen, M.; Kuemmeth, F.; Jespersen, T. S.; Nygård, J.; Krogstrup, P.; Marcus, C. M. Exponential Protection of Zero Modes in Majorana Islands. *Nature* **2016**, *531*, 206.

(10) Deng, M. T.; Vaitiekėnas, S.; Hansen, E. B.; Danon, J.; Leijnse, M.; Flensberg, K.; Nygård, J.; Krogstrup, P.; Marcus, C. M. Majorana bound state in a coupled quantum-dot hybrid-nanowire system. *Science* **2016**, *354*, 1557.

(11) Kang, J. H.; Grivnin, A.; Bor, E.; Reiner, J.; Avraham, N.; Ronen, Y.; Cohen, Y.; Kacman, P.; Shtrikman, H.; Beidenkopf, H. Robust epitaxial Al coating of reclined InAs nanowires. *Nano Lett.* **2017**, *17*, 7520.

(12) Takei, K.; Fang, H.; Kumar, S. B.; Kapadia, R.; Gao, Q.; Madsen, M.; Kim, H. S.; Liu, C.-H.; Chueh, Y.-L.; Plis, E.; Krishna, S.; Bechtel, H. A.; Guo, J.; Javey, A. Quantum confinement effects in nanoscale-thickness InAs membranes. *Nano Lett.* **2011**, *11*, 5008.

(13) Rogers, J. A.; Lagally, M. G.; Nuzzo, R. G. Synthesis, assembly and applications of semiconductor nanomembranes. *Nature* **2011**, *477*, 45.

(14) Suominen, H. J.; Kjaergaard, M.; Hamilton, A. R.; Shabani, J.; Palmstrøm, C. J.; Marcus, C. M.; Nichele, F. Zero-energy modes from coalescing nndreev states in a two-dimensional semiconductor-superconductor hybrid platform. *Phys. Rev. Lett.* **2017**, *119*, 176805.

(15) Ko, H.; Takei, K.; Kapadia, R.; Chuang, S.; Fang, H.; Leu, P. W.; Ganapathi, K.; Plis, E.; Kim, H. S.; Chen, S.-Y.; Madsen, M.; Ford, A. C.; Chueh, Y.-L.; Krishna, S.; Salahuddin, S.; Javey, A. Ultrathin compound semiconductor on insulator layers for high-performance nanoscale transistors. *Nature* **2010**, *468*, 286.

(16) Conesa-Boj, S.; Russo-Averchi, E.; Dalmau-Mallorqui, A.; Trevino, J.; Pecora, E. F.; Forestiere, C.; Handin, A.; Ek, M.; Zweifel, L.; Wallenberg, L. R.; Rüffer, D.; Heiss, M.; Troadec, D.; Dal Negro, L.; Caroff, P.; i Morral, A. F. Vertical "III–V" V-shaped nanomembranes epitaxially grown on a patterned Si [001] substrate and their enhanced light scattering. *ACS Nano* **2012**, *6*, 10982.

(17) Chi, C. Y.; Chang, C. C.; Hu, S.; Yeh, T. W.; Cronin, S. B.; Dapkus, P. D. Twin-free GaAs nanosheets by selective area growth: Implications for defect-free nanostructures. *Nano Lett.* **2013**, *13*, 2506.

(18) Arab, S.; Chi, C. Y.; Shi, T.; Wang, Y.; Dapkus, D. P.; Jackson, H. E.; Smith, L. M.; Cronin, S. B. Effects of surface passivation on twin-free GaAs nanosheets. *ACS Nano* **2015**, *9*, 1336.

(19) Tutuncuoglu, G.; de la Mata, M.; Deiana, D.; Potts, H.; Matteini, F.; Arbiol, J.; i Morral, A. F. Towards defect-free 1-D GaAs/AlGaAs heterostructures based on GaAs nanomembranes. *Nanoscale* **2015**, *7*, 19453.

(20) Soo, M. T.; Zheng, K.; Gao, Q.; Tan, H. H.; Jagadish, C.; Zou, J. Mirror-twin induced bicrystalline InAs nanoleaves. *Nano Res.* **2016**, *9*, 766.

(21) Pan, D.; Fu, M. Q.; Yu, X. Z.; Wang, X. L.; Zhu, L. J.; Nie, S. H.; Wang, S. L.; Chen, Q.; Xiong, P.; von Molnár, S.; Zhao, J. H. Controlled synthesis of phase-pure InAs nanowires on Si (111) by diminishing the diameter to 10 nm. *Nano Lett.* **2014**, *14*, 1214.

(22) Hallberg, R. T.; Messing, M. E.; Dick, K. A. Nanowire morphology and particle phase control by tuning the In concentration of the foreign metal nanoparticle. *Nanotechnology* **2019**, *30*, 054005.

(23) Caroff, P.; Dick, K. A.; Johansson, J.; Messing, M. E.; Deppert, K.; Samuelson, L. Controlled polytypic and twin-plane superlattices in III–V nanowires. *Nat. Nanotechnol.* **2009**, *4*, 50.

(24) Dick, K. A.; Caroff, P. Metal-seeded growth of III–V semiconductor nanowires: towards gold-free synthesis. *Nanoscale* **2014**, *6*, 3006.

(25) Hjort, M.; Lehmann, S.; Knutsson, J.; Zakharov, A. A.; Du, Y. A.; Sakong, S.; Timm, R.; Nylund, G.; Lundgren, E.; Kratzer, P.; Dick, K. A.; Mikkelsen, A. Electronic and structural differences between wurtzite and zinc blende InAs nanowire surfaces: experiment and theory. *ACS Nano* **2014**, *8*, 12346.

(26) Stiles, M. D.; Hamann, D. R. Electron transmission through silicon stacking faults. *Phys. Rev. B: Condens. Matter Mater. Phys.* **1990**, *41*, 5280.

(27) Stiles, M. D.; Hamann, D. R. Ballistic electron transmission through interfaces. *Phys. Rev. B: Condens. Matter Mater. Phys.* **1988**, *38*, 2021.

(28) Joyce, H. J.; Wong-Leung, J.; Gao, Q.; Tan, H. H.; Jagadish, C. Phase perfection in zinc blende and wurtzite III–V nanowires using basic growth parameters. *Nano Lett.* **2010**, *10*, 908.

(29) Zhou, C.; Zheng, K.; Lu, Z. Y.; Zhang, Z.; Liao, Z. M.; Chen, P. P.; Lu, W.; Zou, J. Quality control of GaAs nanowire structures by limiting As flux in molecular beam epitaxy. *J. Phys. Chem. C* **2015**, *119*, 20721.

(30) Wang, Q. H.; Kalantar-Zadeh, K.; Kis, A.; Coleman, J. N.; Strano, M. S. Electronics and optoelectronics of two-dimensional transition metal dichalcogenides. *Nat. Nanotechnol.* **2012**, *7*, 699.

(31) Li, L. K.; Yu, Y. J.; Ye, G. J.; Ge, Q. Q.; Ou, X. D.; Wu, H.; Feng, D. L.; Chen, X. H.; Zhang, Y. B. Black phosphorus field-effect transistors. *Nat. Nanotechnol.* **2014**, *9*, 372.

(32) Pan, D.; Fan, D. X.; Kang, N.; Zhi, J. H.; Yu, X. Z.; Xu, H. Q.; Zhao, J. H. Free-standing two-dimensional single-crystalline InSb nanosheets. *Nano Lett.* **2016**, *16*, 834.

(33) de la Mata, M.; Leturcq, R.; Plissard, S. R.; Rolland, C.; Magén, C.; Arbiol, J.; Caroff, P. Twin-induced InSb nanosails: A convenient high mobility quantum system. *Nano Lett.* **2016**, *16*, 825.

(34) Karataev, V. V.; Mil'vidskiǐ, M. G.; Rytova, N. S.; Fistul', V. I. Compensation in n-type InAs. *Sov. Phys. Semicond.* **1977**, *11*, 1009.

(35) Nainani, A.; Bennett, B. R.; Brad Boos, J.; Ancona, M. G.; Saraswat, K. C. Enhancing hole mobility in III–V semiconductors. *J. Appl. Phys.* **2012**, *111*, 103706.

(36) Boland, J. L.; Amaduzzi, F.; Sterzl, S.; Potts, H.; Herz, L. M.; i Morral, A. F.; Johnston, M. B. High electron mobility and insights into temperature-dependent scattering mechanisms in InAsSb nanowires. *Nano Lett.* **2018**, *18*, 3703.